EFFECTS OF INJECTOR GEOMETRY ON CRYOGENIC COAXAIL JETS AT SUPERCRITICAL PRESSURES

Hiroumi Tani
Department of Aeronautics and Astronautics, School of Engineering, The University of Tokyo
7-3-1 Hongo, Bunkyo-ku Tokyo,113-8656, JAPAN

ABSTRACT

The effects of LOX post recess length and exit taper on the mixing characteristics of coaxial jets, such as the inner-jet-core length and jet spread angle, were investigated under supercritical pressures. In experiments, cryogenic nitrogen/gaseous helium coaxial jets were visualized using the shadowgraph technique. The LOX post recess enhanced the mixing of the inner nitrogen jet when its length was longer than one LOX post exit diameter. The outer helium jet was expanded as the recess length increased. The LOX post exit taper also had significant effects on the mixing of the nitrogen jet and the spread angle of the helium jet. In addition to these injector geometry effects, it is also noted that the inner nitrogen jet had sinusoidal structures. Numerical simulations revealed that large-scale instabilities of nitrogen jets correspond to shear layer instabilities. The large-scale instabilities had the effect of spreading the mixing layer of N_2/He.

1. INTRODUCTION

Most high-thrust liquid oxygen (LOX)/gaseous hydrogen (GH_2) rocket engines operate at combustor pressure above the critical pressure of oxygen (5.04 MPa). Under such supercritical pressures, the oxygen in a combustor no longer experiences atomization but, rather, diffuses directly through turbulent mixing owing to the diminishment of surface tension and liquid/gas phase changes. [1-4]

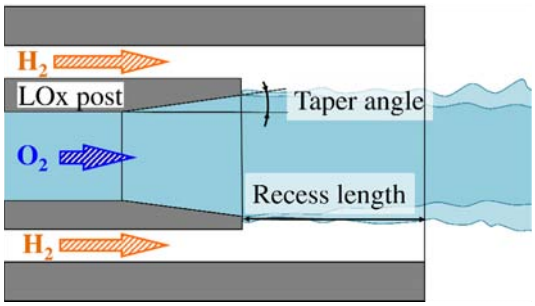

Fig. 1. Design parameters of coaxial injector

Therefore, when designing coaxial injectors for supercritical pressures, injectors should be evaluated by hot-fire and cold-flow tests or numerical simulations under supercritical pressure conditions, rather than by those under subcritical pressures. However, the current standard design procedure for coaxial injectors under supercritical pressures is often strongly dependent on liquid atomization tests at subcritical pressures, such as water/air injection tests. This dependence persists because our knowledge about O_2/H_2 coaxial injection under supercritical pressures is still very limited. It is, therefore, necessary to investigate detailed flow fields of O_2/H_2 coaxial jets at supercritical pressures.

For a more reasonable design procedure for supercritical pressure, it is important to understand the influence of injector geometry upon combustor performance under supercritical conditions. A LOX post recess length is one of the most important parameters of injector geometry. The LOX post is the inner tube of a coaxial injector. Fig. 1 defines LOX post recess length as the axial distance between the exit plane of the LOX post and the injector. Many LOX/GH_2 rocket engines employ coaxial injectors with a recess length equal to the inner diameter of the LOX post. This design has been found to improve atomization and mixing of liquid jets in cold-flow tests under subcritical conditions [5-7]. In hot-fire tests under subcritical pressures [8-10], it has been reported that the LOX post recess has a significant effect on flame spread of O_2/H_2 coaxial jets, thereby yielding improvements in combustion efficiency and stability. The recess effect is, therefore, advantageous for combustor performance under subcritical pressures; however, the recess effect still needs to be carefully checked in the case of supercritical pressures. For instance, Candel et al. [2] and Lux et al. [11] reported that the recess enlarged the flame width, and Woodward et al. [12] observed no improvement in combustion efficiency. It is, thus, important to take into account the difference in the diffusion characteristics of

the oxygen jets between sub- and supercritical pressures in order to understand recess effects under supercritical pressures.

In recent years, there have been extensive efforts to investigate the influence of the recess on O_2/H_2 coaxial jets under supercritical pressures. Candel et al. [2] showed that the LOX post recess induces wake-like instabilities of the dense oxygen jet. Kim et al. [14, 15] conducted numerical simulations and suggested that the recess length influences hydrodynamic instabilities in the recess region.

Effects of other parameters of injector geometry, such as taper angle and wall thickness at the LOX post exit, are also important. The exit taper angle of the LOX post is the inclination of the LOX post inner wall at the exit. Nunome et al. [13] reported that a LOX post exit taper influenced characteristics of combustion instability in an O_2/H_2 combustor.

In order to develop a better understanding of injector geometry effects, the influence on the mixing and unsteady behavior of coaxial jets should be noted, because it is well-known that injector geometry significantly influences combustion efficiency and stability.

The purpose of this study is to investigate injector geometry effects on mixing and unsteady behavior of coaxial jets at supercritical pressures by means of experiments and numerical simulations. In the present work, coaxial jets composed of cryogenic nitrogen (N_2) and gaseous Helium (He) are employed, replacing O_2/H_2 coaxial jets. Mayer et al. [1] have already shown that cryogenic N_2/He coaxial jets at supercritical pressures of nitrogen have mixing characteristics similar to O_2/H_2 coaxial jets at supercritical pressures of oxygen [16, 17]. Moreover, under subcritical pressure conditions, recess effects have been observed in cold-flow tests [5–7]. Therefore, it seems reasonable to begin with non-reacting coaxial jets at supercritical pressures to understand injector geometry effects. This paper first presents results of injection tests. Through experiments, we describe the flow-field features of cryogenic coaxial jets under supercritical pressures. Then, the effects of the LOX post recess length and exit taper angle upon the mixing of coaxial jets are examined. Finally, the results of numerical simulations are shown to investigate in detail the unsteady flow field of cryogenic coaxial jets under supercritical pressures.

2. EXPERIMENTAL ANALYSIS

2.1 Experimental setup and conditions

A schematic diagram of the experimental setup is shown in Fig. 2. The test stand consists of a LN_2 pressurized reservoir, a coaxial injector, a high-pressure chamber, and a supply system for high-pressure N_2 and He gases. Liquid nitrogen is first pressurized to a required level by high-pressure nitrogen gas, then it is injected at a supercritical pressure and a cryogenic temperature into the high-pressure chamber filled with nitrogen gas. Helium gas is supplied to the coaxial injector via a needle valve that controls the flow rate of helium gas. The high-pressure chamber has four windows for optical access, and it is designed to tolerate a maximum pressure of 5 MPa.

The coaxial injector is placed in the upper part of the high-pressure chamber. Injector details are shown in Fig. 3. The injector is about half the size of practical rocket engine injectors. Recess length and exit taper angle of the coaxial injector can be varied in the range 0–6 mm and 0–10° by replacing parts of the injector. In the present study, three different recess lengths (L_{recess}) of 0, 2, 4 mm and two LOX post-exit taper angles (θ_{taper}) of 0° and 9.7° are used. The recess length of 2 mm is equal to the inner diameter of the LOX post with an exit taper angle of 0°. Wall thickness of the LOX post exit decreases as the exit taper angle increases.

Table 1 illustrates typical test conditions. The ratio of the chamber pressure to the critical pressure of nitrogen (3.40 MPa) is about 1.18. The injection temperature of nitrogen is below the critical temperature of nitrogen (126.2 K), as is typical for oxygen in liquid rocket engines. The mass flow rates of cryogenic nitrogen are set to be the same in all injector geometry cases in order to investigate the effects of injector geometry on the mixing of N_2/He.

2.2 Image acquisition and analysis

In order to examine the flow-field features and the mixing of N_2/He coaxial jets at supercritical pressures, instantaneous and time-averaged shadowgraph images are obtained. The shadowgraph technique is commonly used both in hot-fire tests [1, 2, 12] and in cold-flow tests [16, 17] under sub- and supercritical pressures. Instantaneous images are taken using a high-speed shutter camera at a shutter speed of 3 μsec. Time-averaged shadowgraph images are taken at a shutter speed of 0.25 sec.

Mixing degrees of N_2/He coaxial jets are evaluated using normalized luminosity distributions of the time-averaged images. Fig. 4 is an example of the normalized luminosity contours of the time-averaged shadowgraph images. Normalized luminosity in the region just behind the LOX post exit is set to be 1, and that of the background of a coaxial jet is set to be 0.

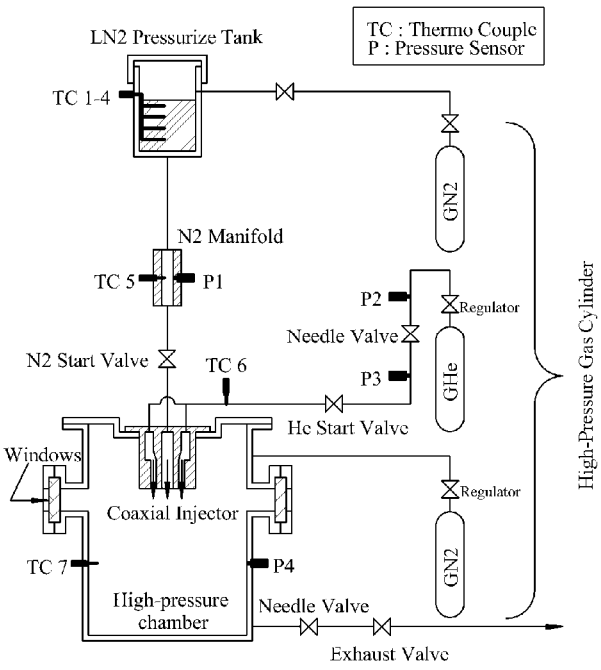

Fig. 2. Simplified diagram of experimental setup.

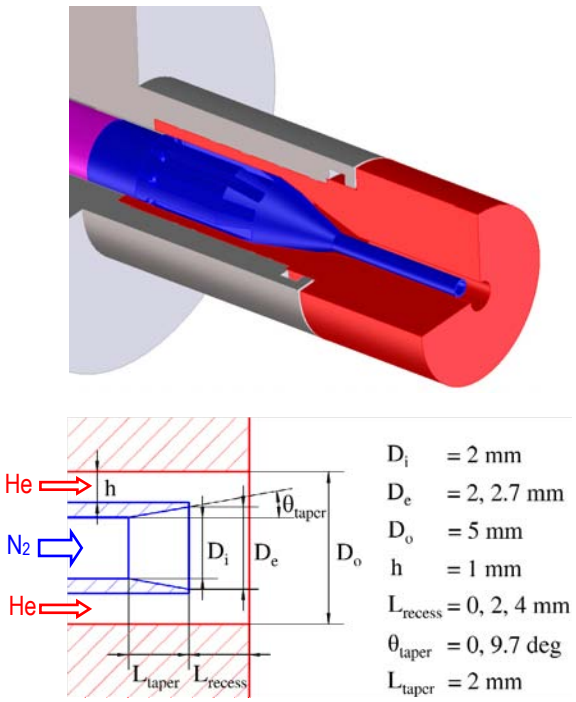

Fig. 3. Schematic of coaxial injector assembly.

Table 1. Typical test conditions.

θ_{taper}		0 deg,	9.7 deg
Chamber pressure, P_{ch}		4.0 MPa	
Chamber temperature, T_{ch}		290 K	
Nitrogen	velocity, V_{N2}	7-8 m/s	4-4.5 m/s
	temperature, V_{N2}	90-100 K	
	Re_{N2} (= $\rho V D_e/\mu$)	1×10^5	7×10^4
Helium	velocity, V_{He}	70-75 m/s	
	temperature, V_{He}	290 K	
	Re_{N2} (= $\rho V h/\mu$)	2.3×10^4	
Density ratio, ρ_{N2}/ρ_{He}		110	
Velocity ratio, V_{He}/V_{N2}		9-10	15-18
Momentum flux ratio, $(\rho V^2)_{He}/(\rho V^2)_{N2}$		0.8-0.9	2.0-3.0

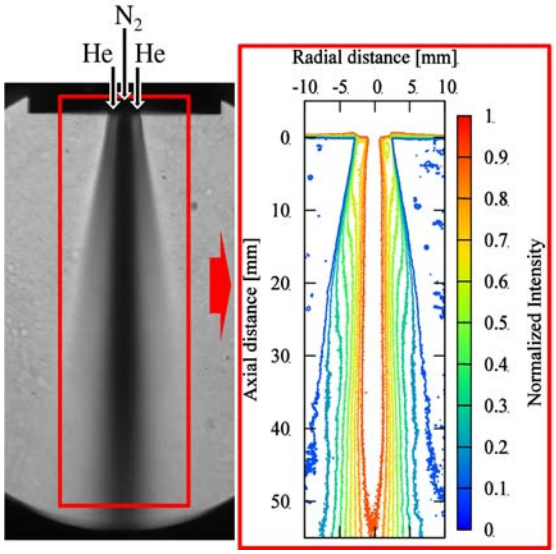

Fig. 4. An example of Nitrogen/Helium coaxial jets: time-averaged shadowgraph original image (left) and normalized luminosity contours (right).

3. EXPERIMENTAL RESULTS

3.1 Flow-field features of cryogenic coaxial jets at supercritical pressures

Firstly, we examined flow-field features of N_2/He coaxial jets at supercritical pressures. Figs. 5a-5c illustrate instantaneous shadowgraph images of N_2/He coaxial jets for three different injector geometry cases. Fig. 5a is the image without the LOX post recess and exit taper. Fig. 5b is the image with a 2-mm-length recess. Fig. 5c is the image with a 9.7° exit taper. For comparison, the image of a N_2 single-hole jet is shown in Fig. 5d. Test conditions for Figs. 5a–5d are given in Table 2.

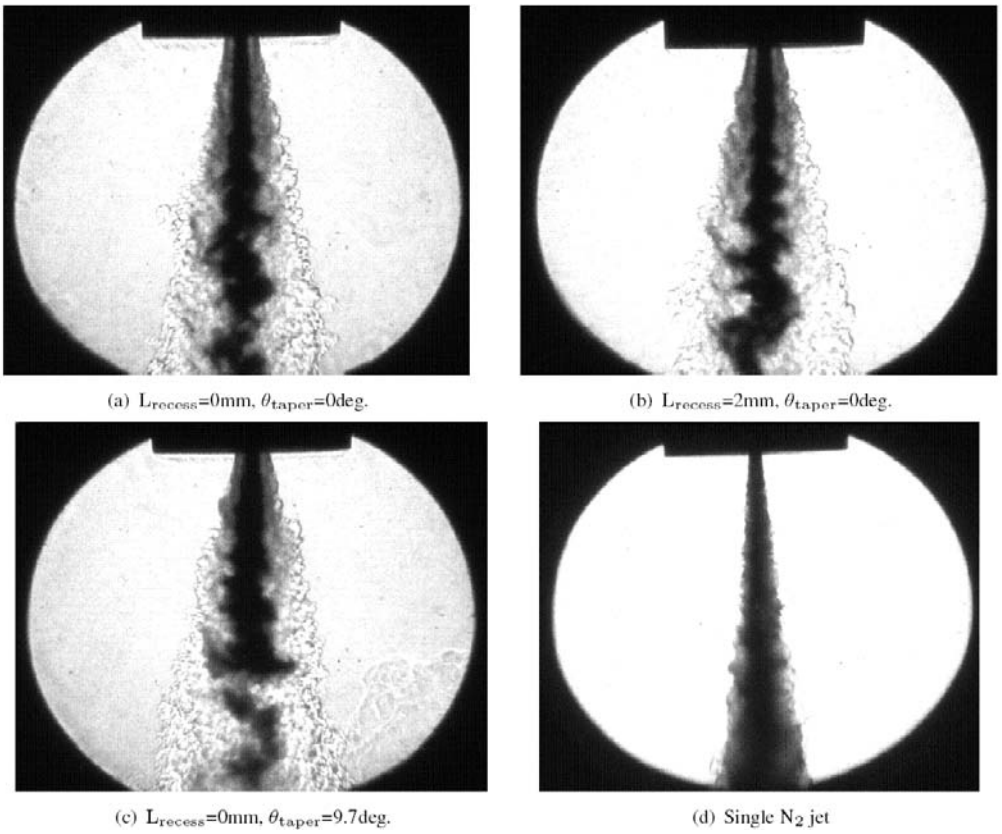

Fig. 5. Instantaneous shadowgraph images of N_2/He coaxial jets (a)-(c) and N_2 single jet (d).

Table 2. Test conditions of coaxial jets in Figs. 5 and 6.

	V_{N2}, m/s	V_{He}, m/s	T_{N2}, K	T_{He}, K
Fig. 5a	8.1	75.0	105.7	293.9
Fig. 5b	7.6	73.1	100.1	292.2
Fig. 5c	4.4	71.1	97.9	292.6
Fig. 5d	8.8	-	103.1	-
Fig. 6a	7.7	72.6	106.5	293.6
Fig. 6b	7.4	71.0	95.0	290.9
Fig. 6c	7.8	71.3	93.3	294.7
Fig. 6d	4.1	71.6	100.5	294.1
Fig. 6e	4.1	70.3	88.0	292.1
Fig. 6f	4.2	72.3	93.8	294.0

As shown in Figs. 5a–5c, a dark region exists near the central axis of the injector. In hot-fire tests of O_2/H_2 coaxial injection [12, 18-20], this dark region has been also observed; it is referred to as the “LOX core” or “dark core” that is due to the presence of dense oxygen. Correspondingly, the dark region seen in

Fig. 5 is considered as the dense nitrogen. Therefore, in the present study, this dark region is called “nitrogen core”. The gray region around the dark core in Fig. 5 is regarded as the helium jet.

Focusing on the behavior of the nitrogen core in Figs. 5a–5c, it appears that the dense nitrogen does not experience an atomization process but, rather, diffuses directly through turbulent process, as reported in past studies on coaxial jets under supercritical pressures [16, 17, 20]. In the mixing layer between the nitrogen core and its ambient fluids, the dense nitrogen has a cloud-like appearance.

Moreover, we note that the nitrogen core of coaxial jets has sinusoidal (possibly helical in three dimension) structures, as shown in Figs. 5a–5c. These structures are observed in all geometrical cases of coaxial jets, but they do not appear in any case of N_2 single-hole jets, as shown in Fig. 5d. Thus, the sinusoidal structures of the nitrogen core are induced by the presence of the outer helium jets. Frequencies of the sinusoidal oscillations are estimated to be about 1–10 kHz from the injection velocities (about 7–70 m/s) and the visible wavelength (about 5 mm). Habiballah et al. [3] and Woodward et al. [12] reported that the LOX core shows the similar sinusoidal oscillations in hot-fire tests at supercritical pressures. Because the behavior of the LOX core is considered to be related to combustion instability in rocket engine combustors [14, 15], it is important to analyze the sinusoidal structures of the dark core. In Section 4, we numerically investigate the unsteady behavior of N_2/He coaxial jets.

3.2 Geometry effects on dark-core length

Dark-core length is one of the indicators of the mixing of coaxial jets at supercritical pressures [18, 20]. Therefore, we compared nitrogen core lengths in order to examine the effects of injector geometry on mixing of N_2/He coaxial jets. Fig. 6 shows normalized luminosity contours of the time-averaged shadowgraph images in six different geometry cases. Test conditions of Fig. 6 are illustrated in Table 2.

In those cases without the exit taper (see Figs. 6a-6c), nitrogen-core (dark-core) length decreases as recess length increases. The same tendency is apparent in the cases of 9.7° exit taper (see Figs. 6d-6f). For proper comparison, the normalized luminosity profiles along the jet center line are illustrated in Fig. 7. (Note that the abscissa is the axial distance from the LOX post-exit plane.) Figs. 7a and 7b are the profiles in the cases without the exit taper and with a 9.7° exit taper, respectively.

In Fig. 7a, the nitrogen-core lengths with 2-mm and 4-mm recess lengths are shorter than those in the absence of the recess. These decreases in nitrogen-core length imply that the recess has the effect of enhancing the mixing of N_2/He coaxial jets. In the cases with a 9.7° exit taper, the 4-mm length recess also improves the mixing but the 2-mm length recess has no effect on the mixing, as shown in Fig. 7b. These results suggest that a certain length of the recess is required to improve the mixing of coaxial jets at supercritical pressures, and that the minimum length to obtain the recess effect is dependent on the injection conditions and the other parameters of the injector geometry, such as LOX post-exit taper.

The effects of the LOX post-exit taper on the mixing of N_2/He coaxial jets are very significant. As shown in Fig. 6, the nitrogen cores with the LOX post-exit taper are shorter and wider than those without the exit taper. In the present study, the injection velocity of nitrogen in the cases of 9.7° exit taper is smaller than that in the absence of the exit taper, because the mass flow rates of nitrogen are set to be the same in all geometry cases. Hence, it is suggested that the increase in the injection velocity ratio of helium and nitrogen (V_{He}/V_{N2}) is one of the major factors likely to improve the mixing of N_2/He coaxial jets.

3.3 Geometry effects on jet spread angle

The spread angle of the helium jet is also strongly influenced by the LOX post recess and exit taper. Fig. 8 shows the changes in the spread angle of the helium jet with the recess length. The spread angles in Fig. 8 are measured using the images in Fig. 6 by setting the threshold luminosity to 0.05. Fig. 8 shows that, upon increasing the recess length or the exit taper angle, the spread angle of the helium jet increases. This effect of the injector geometry on the jet spread angle can be one of the factors that account for the increase in the flame expansion of O_2/H_2 coaxial jets reported in hot-fire tests [1, 2]. Hence, it is noteworthy that the spread angle of the helium jet is determined not only by the injection velocity of helium, but also by the recess length and the taper exit angle.

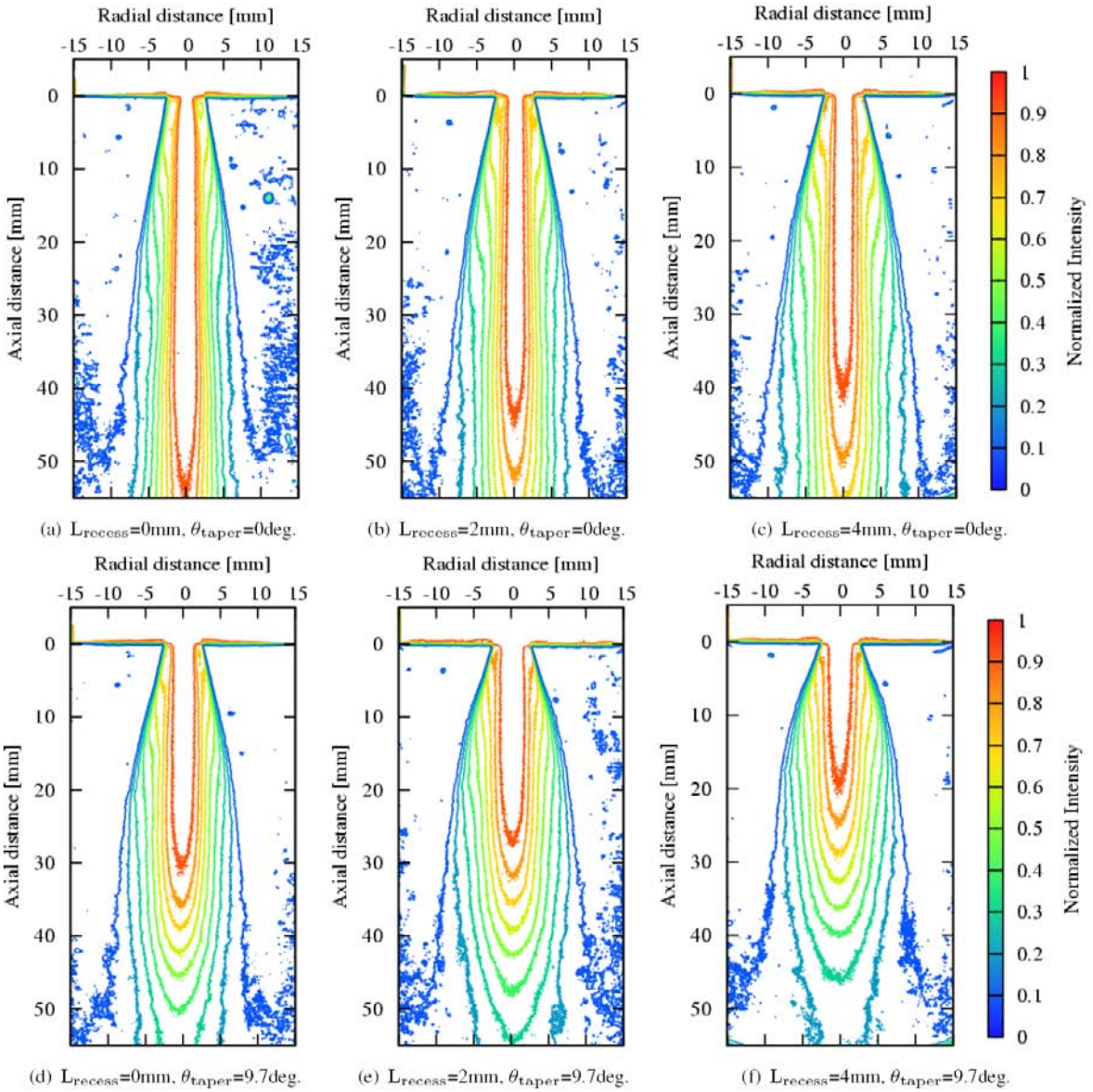

Fig. 6. Normalized luminosity contours of N_2/He coaxial jets.

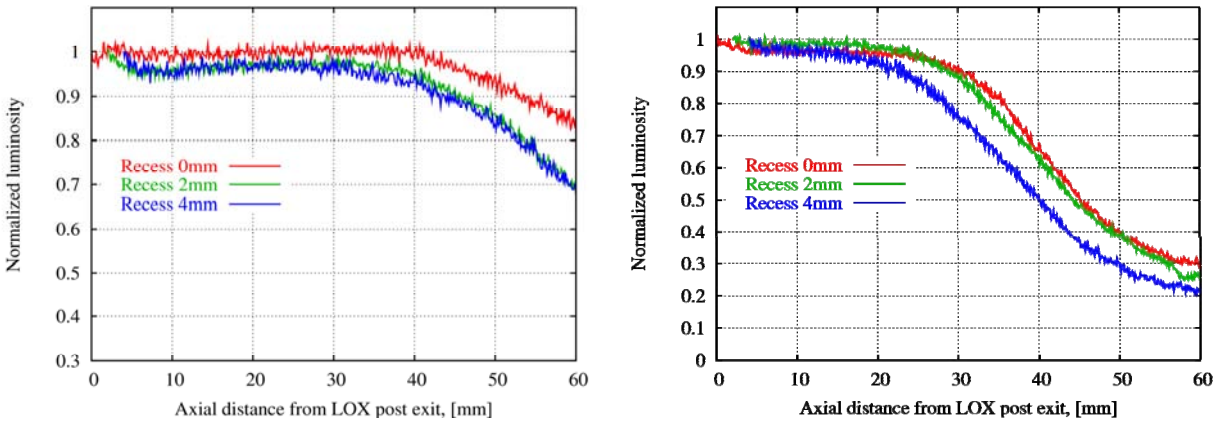

(a) θ_{taper} = 0 deg. (b) θ_{taper} = 9.7 deg.

Fig. 7. Normalized luminosity of time-averaged shadowgraph images along N_2 jet center line.

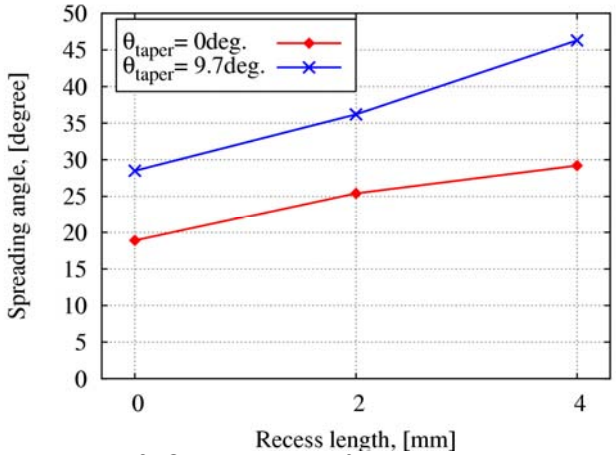

Fig. 8. Spread angle of outer helium jets.

4. NUMERICAL ANALYSIS

The flow-field features of cryogenic N_2/He coaxial jets under supercritical pressures were further investigated in detail through numerical simulations, focusing mainly on the unsteady behavior of the nitrogen jet.

4.1 Governing equations and thermodynamic properties

The governing equations are the three dimensional compressible Reynolds-averaged Navier-Stokes (RANS) equations. Turbulent viscosity was modelled by the Menter Shear Stress Transport model [21]. The turbulent Prandtl number and the turbulent Schmidt number are both assumed to be constant and equal to 0.8.

The governing equations are solved using the preconditioning scheme [22] to accelerate the convergence in the simulations of low-mach number flows. Numerical fluxes for the convective terms are evaluated by the preconditioned Roe's scheme with the MUSCL interpolation. In the steady-state simulation, the preconditioned LU-SGS scheme is employed for time integration. In the unsteady simulation, a dual time-stepping integration algorithm [23] is incorporated into the preconditioning scheme by adding a pseudotime term to the governing equations. The inner-loop pseudo-time term is integrated with the LU-SGS scheme. The physical-time term is discretized using a second-order backward difference.

The equation of state employed here is the Soave-Redlich-Kwong equation of state [24], which can be applied over broad temperature and pressure ranges. The van der Waals mixing rules are used to calculate the properties of nitrogen/helium mixtures [24]. The thermodynamic properties such as speed of sound and specific enthalpy are derived from the equation of state using thermodynamic relational expressions. Transport properties, including viscosity and thermal conductivity, are obtained using the methodology of Chung et al. [24]. Mass diffusivity at high pressures is calculated by the method of Riazi et al. [25].

4.2 Validation of numerical model

Numerical schemes in the present model are validated for a cryogenic nitrogen jet at a supercritical pressure. The reference test case is an experiment (RCM1A test case) conducted by Mayer et al. [16]. Density profiles were measured using Raman diagnostics. Cryogenic nitrogen at a temperature of 126.9 K was injected into gaseous nitrogen at a supercritical pressure (4 MPa) and ambient temperature (298 K). The injector configuration is illustrated in Fig. 9. The computational domain is a cylindrical sector for an axisymmetric calculation, and it encompasses a chamber region with a total of 421×166 grid points on an x-z plane.

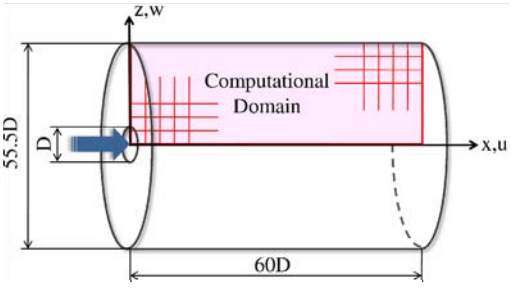

Fig. 9. Configuration of RCM1A test case; D = 2.2 mm is diameter of injector hole.

Direct comparisons between measured and calculated results are shown in Fig. 10. The k-ε computational results by Cheng et al. [26] are also plotted in Fig. 10. Results calculated using our current numerical model agree well with the experimental data. Thus, it can be confirmed that our proposed model properly simulates cryogenic jets under supercritical pressures.

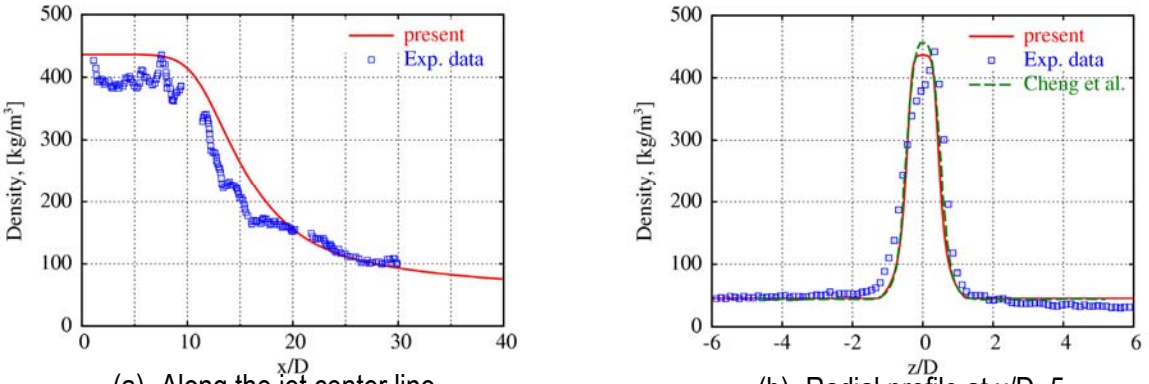

(a) Along the jet center line (b) Radial profile at x/D=5

Fig. 10. Calculated density profiles compared with experimental data.

4.3 Unsteady RANS simulation of cryogenic N_2/He coaxial jet

A schematic of the computational domain is shown in Fig. 11. The computational domain is a cylindrical sector for a quasi-2D calculation, and it consists of an axisymmetric coaxial injector region and a downstream chamber region with a total of 85,139 grid points on an x-z plane. The geometry of the coaxial injector matches that of the test injector without the LOX post recess and exit taper in experiments.

The boundary conditions are as follows: At the inlet boundaries of the inner and outer tube of the injector, the pressure, temperature, and velocity are specified in Table 3. On the injector face plate, nonslip adiabatic conditions are imposed. At the downstream boundary of the cylindrical chamber, nonreflecting boundary conditions, based on the method of characteristics, are applied [27]. A periodic condition is applied in the azimuthal direction.

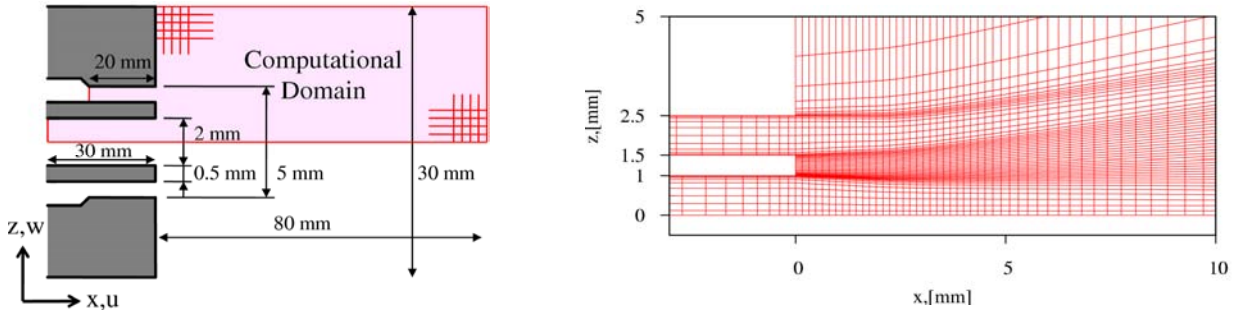

(a) Coaxial injector dimensions (b) Computational mesh near the injector

Fig. 11. Schematic diagram of computational domain.

Fig. 12 shows instantaneous profiles of density and temperature for the case of unsteady RANS (URANS). The nitrogen jet appears to have a large-scale instability, with wavelengths comparable to the sinusoidal instabilities observed in experiments. The large-scale instability of the nitrogen jet can be regarded as Kelvin-Helmholtz instability induced by the N_2/He shear layers. Fig. 13 presents frequency spectra of density oscillation at the location indicated by the "Probe" in Fig. 12a. The dominant frequency of the large-scale instability of the nitrogen jet is about 3.65 kHz.

In order to investigate the influence of the large-scale instability of the nitrogen jet on the mixing of N_2/He coaxial jets, a comparison of time-averaged density profiles between the URANS and steady RANS results is shown in Fig. 15. Comparing the thickness of the mixing layers, we find that the large-scale instability of the nitrogen jet has the effect of enhancing the mixing of coaxial jets, especially in the vicinity of the injector.

Finally, Fig. 14 gives the density profiles along the center line of the coaxial injector. The potential cores of the nitrogen jet in the case of both URANS and steady RANS are quite a bit shorter than the experimentally

measured nitrogen cores (shown in Fig. 7a). Considering that the current numerical code predicted the core-length quite well, the difference in the core lengths suggests that the dark core visualized in shadowgraph images does not exactly correspond to the potential core of the inner jet of the coaxial jet.

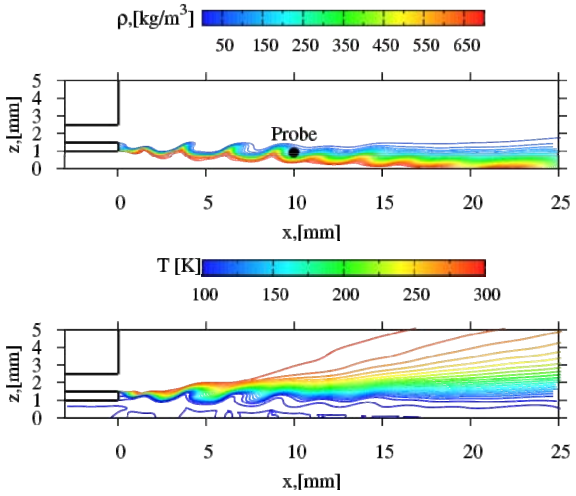

Fig. 12. Snapshots of density and temperature of N_2/He coaxial jet.

Table 3. Injection conditions in numerical simulations.

P [MPa]	4.0
$T_{ambient}$ [K]	295
T_{N2} [K]	100
ρ_{N2} [kg/m^3]	695.5
V_{N2} [m/s]	8.0
T_{He} [K]	295
ρ_{He} [kg/m^3]	6.4
V_{He} [m/s]	75.0
ρ_{N2} /ρ_{He}	109
$(\rho V^2)_{N2}$ /$(\rho V^2)_{He}$	1.23

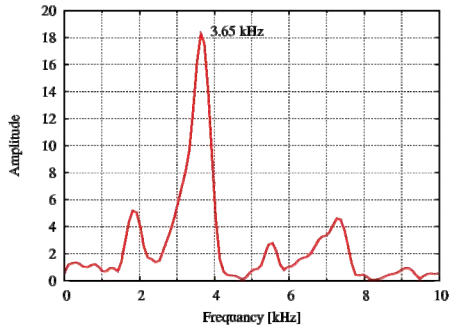

Fig. 13. Frequency spectrum of density oscillation at probe point.

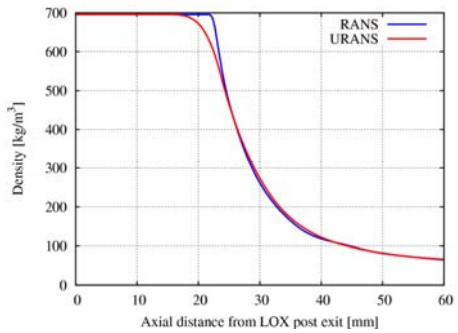

Fig. 14. Density profiles along center line of coaxial injector.

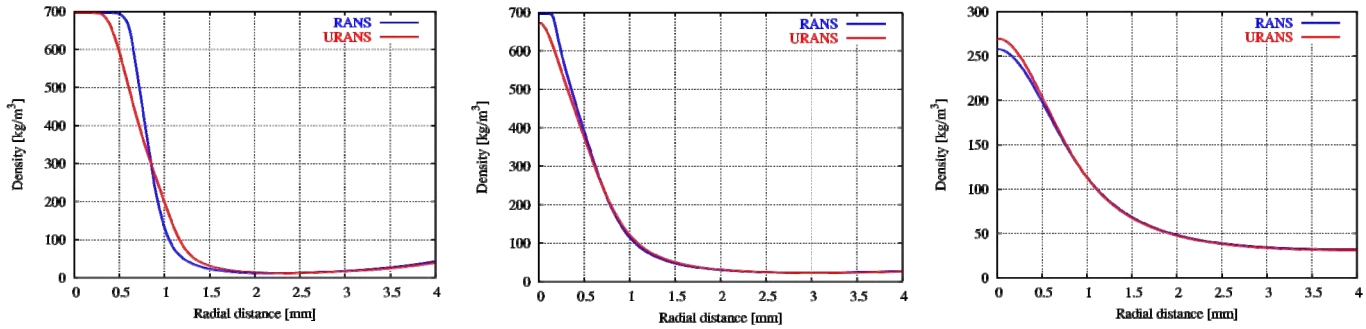

(c) Radial profile at x = 10 mm (b) Radial profile at x = 20 mm (a) Radial profile at x = 30 mm

Fig. 15. Comparison of density profiles between URANS and RNAS.

5. SUMMARY

Cold-flow tests for cryogenic N_2/He coaxial jets were conducted under supercritical pressure conditions in order to investigate the effects of the LOX post recess and exit taper upon the mixing of coaxial jets. Flow-field features of the cryogenic N_2/He coaxial jets under supercritical pressures were also examined experimentally and numerically.

In experiments, the mixing of coaxial jets was evaluated with respect to the dark core lengths obtained from shadowgraph images. As a result, we found that the LOX post recess can enhance the mixing of cryo-

genic coaxial jets at supercritical pressures, when the recess length is sufficiently large. The LOX post exit taper also had significant effects on the mixing of the nitrogen jet. Moreover, both the LOX post recess and exit taper have the effect of enlarging the spread angle of the helium jet.

With regard to flow-field features of cryogenic coaxial jets under supercritical pressures, instantaneous shadowgraph images showed that the inner nitrogen jet had the sinusoidal (possibly helical in three dimension) structures. In unsteady numerical simulations of N_2/He coaxial jets, large-scale instabilities were likewise observed to correspond to shear layer instabilities, which lead to the effect of spreading the mixing layer of N_2/He. Numerical results also suggested that the dark core observed in shadowgraph images does not exactly correspond to the potential core of the inner jet.

ACKNOWLEDGMENT

This work was supported by a Grant-in-Aid from the Japan Society for the Promotion of Science Fellows.

REFERENCES

[1] Mayer W. and Tamura H., Propellant Injection in a Liquid Oxygen/Gaseous Hydrogen Rocket Engine. *Journal of Propulsion and Power*, Vol. 12, No. 6, pp.1137-1147, 1996.
[2] Candel S., Junper M., Singla G., Scouflaire P., and Rolon C., Structure and Dynamics of Cryogenic Flames at Supercritical Pressure. *Combustion Science and Technology*, Vol. 178, pp. 161–192, 2006.
[3] Habiballah M., Orain M., Grisch F., Vingert L., and Gicquel P., Experimental Studies of High-Pressure Cryogenic Flames on the MASCOTTE Facility. *Combustion Science and Technology*, Vol. 178, pp. 101–128, 2006.
[4] Oefelein J., Mixing and Combustion of Cryogenic Oxygen-Hydrogen Shear-Coaxial Jet Flames at Supercritical Pressure. *Combustion Science and Technology*, Vol. 178, pp. 229–252, 2006.
[5] Burick R., Space Storable Propellant Performance Program Coaxial Injector Characterization. NASA CR–120936, 1972.
[6] Mehegan P., Campbell D., and Scheuerman C., Investigation of Gas-Augmented Injectors. NASA CR–72703, 1970.
[7] Gill G. and Nurick W., Liquid Rocket Engine Injectors. NASA SP–8089, 1976.
[8] Hanuum N. and Conrad E., Some Injector Element Detail Effects on Screech in Hydrogen-Oxygen Rockets. NASA TM X–52363, 1967.
[9] Kendrick D., Herding G., Scouflaire P., Rolon C., and Candel S. Effects of a Recess on Cryogenic Flame Stabilization. *Combustion and Flame*, Vol. 118, pp. 327–339, 1999.
[10] Hulka J. and Hutt J., Instability Phenomena in Liquid Oxygen/Hydrogen Propellant Rocket Engines. Liquid Rocket Engine Combustion Instability, pp. 39–71, Progress in Astronautics and Aeronautics, 1995.
[11] Lux J. and Haidn O., Effect of Recess in High-Pressure Liquid Oxygen/Methane Coaxial Injection and Combustion, *Journal of Propulsion and Power*, Vol. 25, No. 1, pp. 24-32, 2009.
[12] Woodward R., Pal S., Farhangi S., Jensen G., and Santoro R. LOX/GH2 Shear Coaxial Injector Atomization Studies: Effect of Recess and Nonconcentricity. AIAA 2007–0571, 2007.
[13] Nunome Y., Takahashi M., Kumakawa A., Miyazaki K., Yoshida S., and Onga T. High-Frequency Flame Oscillation Observed at a Coaxial LOX/LH2 Injector Element. AIAA 2008–4848, 2008.
[14] Kim B. and Heister S., Two-Phase Modelling of Hydrodynamic Instabilities in Coaxial Injectors. *Journal of Propulsion and Power*, Vol. 20, No. 3, pp. 468-479, 2004.
[15] Kim B., Heister S., and Collicott S. Three-Dimensional Flow Simulations in the Recessed Region of a Coaxial Injector. *Journal of Propulsion and Power*, Vol. 21, No. 4, pp. 728–742, 2005.
[16] Branam R. and Mayer W., Characterization of Cryogenic Injection at Supercritical Pressure. *Journal of Propulsion and Power*, Vol. 19, pp. 342–355, 2003.
[17] Leyva I., Chehroudi B., and Talley D. Dark Core Analysis of Coaxial Injectors at Sub-, Near-, and Supercritical pressures in a Transverse Acoustic Field. AIAA 2007–5456, 2007.
[18] Woodward R., Pal S., Farhangi S., Jensen G., and Santoro R. LOX/GH2 Shear Coaxial Injector Atomization Studies at Large Momentum Flux Ratios. AIAA 2006–5203, 2006.
[19] Smith J., Bechle M., Suslov D., Oschwald M., Haidn O., and Schneider G. High-Pressure LOx/H2 Combustion and Flame Dynamics Preliminary Results. AIAA 2004–3376, 2004.
[20] Davis D. and Chehroudi B., Measurements in an Acoustically Driven Coaxial Jet under Supercritical Conditions. AIAA 2005–736, 2005.
[21] Menter F., Two-Equation Eddy Viscosity Turbulence Models for Engineering Applications, *AIAA Journal*, Vol. 36, No. 9, pp. 1610-1617, 1998.
[22] Weiss J. and Smith W., Preconditioning Applied to Variable and Constant Density Flows, *AIAA Journal*, Vol. 33, pp.2050-2056, 1995.
[23] Shuen J., Chen K., and Choi Y., A Coupled Implicit Method for Chemical Nonequilibrium Flows at All Speeds, *Journal of Computational Physics*, Vol. 106, pp.306-318, 1993.
[24] Poling B., Prausnitz J., and O'Connell J., The Properties of Gases and Liquids, McGraw-Hill, 5th ed., 2001.
[25] Riazi. M. and Whitson C., Estimating Diffusion Coefficients of Dense Fluids, *Industrial and Engineering Chemistry Research*, Vol. 32, pp.3081-3088, 1993.
[26] Cheng G. and Farmer R., CFD Spray Combustion Model for Liquid Rocket Engine Injector Analysis, AIAA 2002-0785, 2002.
[27] Okong'o N. and Bellan J., Consistent Boundary Conditions for Multicomponent Real Gas Mixtures Based on Characteristic Waves, *Journal of Computational Physics*, Vol. 176, pp. 330-344, 2002.